Mechanism for strong magnetoelectric coupling in dilute magnetic ferroelectrics

L. Weston,[1] X. Y. Cui,[2,3] S. P. Ringer,[2,3] and C. Stampfl[1]
[1]*School of Physics, The University of Sydney, Sydney, New South Wales 2006, Australia*
[2]*Australian Institute for Nanoscale Science and Technology, The University of Sydney, New South Wales 2006, Australia*
[3]*School of Aerospace, Mechanical and Mechatronic Engineering, The University of Sydney, New South Wales 2006, Australia*
(Received 25 July 2016; published 16 November 2016)

The manipulation of atomic-scale magnetization is important from both a fundamental and a practical perspective. Using first-principles density-functional-theory calculations within the hybrid functional approach, we systematically study spin-lattice coupling effects for isolated $3d^4$–$3d^7$ transition-metal dopants in a nonmagnetic, ferroelectric $PbTiO_3$ host material. When present at the B-site, a low-spin (or intermediate-spin) to high-spin crossover induces marked ferroelectric-like distortions in the local geometry, characterized by a shift of the dopant ion with respect to the surrounding O_6 octahedral cage. The origins of this microscopic multiferroic effect are discussed in terms of the pseudo-Jahn-Teller theory for ferroelectricity. The possibility to exploit this phenomenon to achieve strong magnetoelectric coupling, including controlled spin switching, is also investigated. These results provide a further understanding of ferroelectricity and multiferroicity in perovskite oxides, and they suggest a possible pathway to manipulate single atomic spins in semiconductor solid solutions.

DOI: 10.1103/PhysRevB.94.184419

I. INTRODUCTION

Magnetoelectric multiferroic materials can simultaneously exhibit ferroelectricity and magnetism, with potentially some coupling between the two [1,2]. Such materials are interesting both from a fundamental perspective, due to the interesting physics they display, but also from a practical perspective, since they promise a range of new device functionalities [3,4]. Perhaps the most exciting prospect for multiferroic materials is the electrical control of magnetism, as this is crucial for the development of novel and high-efficiency multiferroic logic devices for data storage and computation [5–8].

Perovskite oxides are among the most promising candidates as multiferroic materials; indeed, the classic ferroelectrics such as $PbTiO_3$ (PTO) and $BaTiO_3$ (BTO) have the tetragonal perovskite structure [9]. However, while many perovskites contain the unpaired d electrons necessary for magnetism, it has become obvious that the presence of d electrons at the B-site cation removes the tendency for a ferroelectric distortion [10,11]. In fact, almost all ferroelectric perovskites have a d^0 cation at the B-site (e.g., Ti^{4+} in PTO and BTO) [12], and this phenomenon has been dubbed the ferroelectric "d^0" rule.

Nevertheless, according to the pseudo-Jahn-Teller (PJT) theory developed by Bersuker, a ferroelectric lattice instability exists for certain d^n B-cations in a perovskite oxide [13]. Moreover, in some cases, the ferroelectric instability is sensitive to the spin state of the B-cation, suggesting a mechanism for strong magnetoelectric coupling, i.e., the multiferroic crossover effect. Using first-principles calculations for model tetragonal structures of $LaBO_3$ perovskites, as well as $BiCoO_3$, we have demonstrated this effect for d^4–d^7 cations in bulk perovskites, and it was shown that a low-spin (LS) to high-spin (HS) crossover can lead to a switching from a paraelectric phase to a ferroelectric phase [11]. Unfortunately, in almost all cases, perovskites with a d^4–d^7 B-cation prefer to undergo competitive centrosymmetric distortions, which reduce or remove the tendency for a polar one [14,15]. One approach to overcome this limitation is to dope a nonmagnetic, ferroelectric material with isolated d^n ($n > 0$) cations at the B-site [16].

Recent advances in the field of solitary dopant electronics (solotronics), particularly with regard to the controlled creation, manipulation, and measurement of isolated dopants, have enabled the development of spintronic devices based on the isolated spins of single dopants [17]. To date, advanced control of isolated spins has been reported for select systems, for example in the optical manipulation of nitrogen-vacancy (NV) centers in diamond, where isolated spins can reportedly be prepared, manipulated, and read out [18]. However, the electrical control of isolated spins could be more appealing, and it could lead the way to simple voltage switching in solotronic devices. If so, electrically controlled spins of isolated dopants, which would represent the extreme microscopic limit of multiferroicity, could provide a pathway to realizing novel electronic and spintronic devices of the future.

Recently, using Co^{3+}-doped PTO as a model system, we demonstrated that switching between the spin states of the Co^{3+} dopant leads to local ferroelectric distortions of the CoO_6 octahedron [16]; moreover, it was demonstrated that by manipulating the ferroelectric polarization, which can potentially be achieved with an applied electric field, spin crossover can be induced [16]. In the present paper, we systematically study the local magnetoelectric properties of Mn, Fe, Co, and Ni transition-metal (TM) dopants in PTO, and we confirm that the multiferroic crossover effect is a general property of d^4–d^7 dopants at the B-site of PTO. For all dopants, a LS to HS crossover leads to an increase in the local ferroelectric character of the dopant BO_6 octahedron. The origins of these effects are explained in detail within the PJT theory for ferroelectricity. Moreover, the dopant HS-LS splitting is sensitive to local geometry, and atomic displacements such as those induced by an external electric field can lead to multiferroic crossover, suggesting a promising route toward strongly coupled multiferroic effects on a truly microscopic scale.

II. METHODOLOGY

Our calculations are performed within the density-functional theory (DFT), using the screened hybrid functional

of Heyd, Scuseria, and Ernzerhof (HSE) [19]. In the hybrid functional calculations, the short-range exchange potential is calculated by mixing a fraction of Hartree-Fock exchange with exchange from a DFT-PBE [20] calculation; unless otherwise noted, we use the standard implementation HSE06—while HSE06, with a mixing parameter of $\alpha = 0.25$, is known to give an excellent account of the atomic and electronic structure, to determine the spin splitting, the mixing parameter is reduced to $\alpha = 0.125$ [21,22] (the spin-state energetics as a function of this mixing parameter is also investigated in detail in Sec. III C). The screening length separating the short-range and long-range exchange potential is set to 10 Å. The valence electrons are separated from the core by use of projector-augmented-wave pseudopotentials (PAWs) [23] as implemented in the VASP package [24]. For the present calculations, Pb $6s^2 6p^2$, Ti $4d^3 5s^1$, Mn $4s^2 3d^5$, Fe $4s^2 3d^6$, Co $4s^2 3d^7$, Ni $4s^2 3d^8$, and O $2s^2 2p^4$ electrons are treated as valence. The energy cutoff for the plane-wave basis set is 500 eV. For the tetragonal five-atom perovskite primitive cells, a $6 \times 6 \times 6$ **k**-point grid is used. For larger supercells, we use an equivalent sampling of the Brillouin zone. Fixed-spin moment calculations are performed so as to study the different spin states of each magnetic transition-metal dopant. In this approach, a self-consistent calculation is carried out under a constrained total magnetic moment. For dilute doping in PTO, a $3a \times 3b \times 3c$ supercell is constructed having 135 atoms in total. A single nonmagnetic Ti atom is replaced by either Mn, Fe, Co, or Ni; the different oxidation states of the dopant atoms are achieved by adding or removing electrons from the supercell with a homogeneous background charge to compensate. As is the typical approach for defect studies based on DFT, the lattice vectors are fixed to the experimental values for tetragonal PTO ($a = 3.904$ Å, $c = 4.1575$ Å [25]) and the internal coordinates are relaxed until the forces are less than 0.01 eV/Å.

III. RESULTS AND DISCUSSION

A. Multiferroic crossover for $3d^4$–$3d^7$ cations

Before presenting our findings, we give a brief introduction to perovskite ferroelectricity and multiferroicity. The unit cells of a perovskite oxide in both the cubic and tetragonal ferroelectric crystal structures are shown in Fig. 1(a). Compared to the cubic phase, the tetragonal ferroelectric structure is characterized by an elongation of the c-axis lattice vector with respect to that of the a axis ($c/a > 1$), as well as a shift of the B-site cation with respect to the oxygen ions in the surrounding O_6 octahedron. The internal shifting of atomic coordinates breaks inversion symmetry and leads to a net macroscopic electrical polarization [9].

The B-site cation in a simple perovskite oxide is sixfold-coordinated to neighboring O atoms in an octahedral geometry. In this octahedral crystal field, the fivefold-degenerate free-ion d band of the B-cation is split into a low-lying triplet of t_{2g} symmetry and a higher-lying doublet of e_g symmetry, as shown in Fig. 1(b). It is a consequence of this splitting that d^4–d^7 ions at the B-site can have their d band filled in either a LS or HS configuration [26], the former being favored by a large splitting and the latter being favored by a large spin-pairing energy and

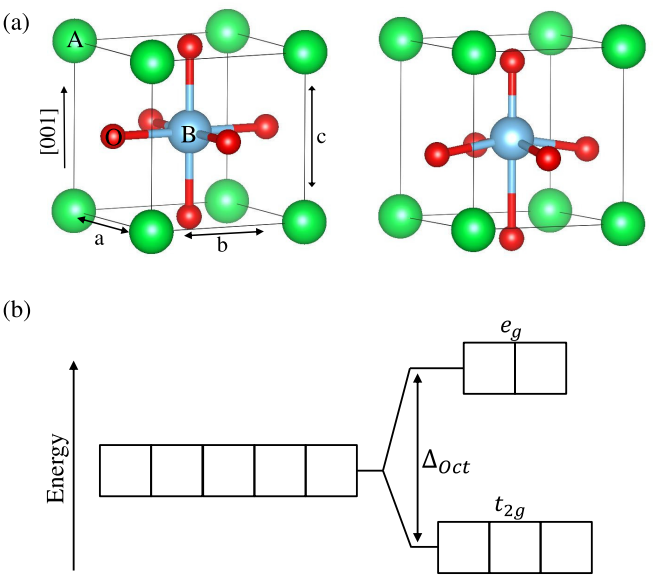

FIG. 1. (a) Unit cell of an ABO_3 perovskite in the cubic (left) and tetragonal ferroelectric (right) structures. With respect to the cubic system, the tetragonal unit cell is characterized by an elongated c-axis lattice vector, and a shift of the B-site cation along the [001] direction with respect to the surrounding oxygen octahedron. Green spheres represent the A-cation, blue the B-cation, and red spheres represent oxygen atoms. (b) In the presence of an octahedral crystal field, the free ion d band of the B-cation is split into a t_{2g} triplet and a higher-lying e_g doublet.

Hund's exchange. In some cases, an intermediate-spin (IS) state is also possible. The LS and HS states of d^4–d^7 B-cations in an octahedral crystal field will maximize and minimize spin pairing, respectively. In Table I, the expected orbital filling for the LS, IS, and HS states is shown for d^4–d^7 B-cations, based on this simple ligand-field model. We note that referring to the antibonding states as a "d-band" is somewhat of a

TABLE I. Electronic configuration (Elec. config.) for each transition-metal ion (TM ion) in either a low-spin (LS), intermediate-spin (IS), or high-spin (HS) state, as predicted from the ligand-field model. The spin quantum number S for each configuration is also shown.

d-filling	Spin state	Elec. config.	S
d^4	LS	$t_{2g}(\uparrow)^3 t_{2g}(\downarrow)^1$	1
	HS	$t_{2g}(\uparrow)^3 e_g(\uparrow)^1$	2
d^5	LS	$t_{2g}(\uparrow)^3 t_{2g}(\downarrow)^2$	1/2
	IS	$t_{2g}(\uparrow)^3 t_{2g}(\downarrow)^1 e_g(\uparrow)^1$	3/2
	HS	$t_{2g}(\uparrow)^3 e_g(\uparrow)^2$	5/2
d^6	LS	$t_{2g}(\uparrow)^3 t_{2g}(\downarrow)^3$	0
	IS	$t_{2g}(\uparrow)^3 t_{2g}(\downarrow)^2 e_g(\uparrow)^1$	1
	HS	$t_{2g}(\uparrow)^3 t_{2g}(\downarrow)^1 e_g(\uparrow)^2$	2
d^7	LS	$t_{2g}(\uparrow)^3 t_{2g}(\downarrow)^3 e_g(\uparrow)^1$	1/2
	HS	$t_{2g}(\uparrow)^3 t_{2g}(\downarrow)^2 e_g(\uparrow)^2$	3/2

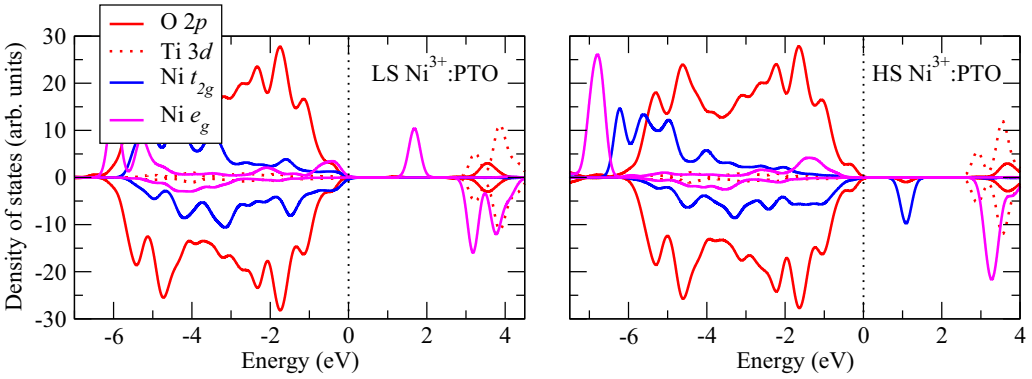

FIG. 2. The partial and projected density of states (PDOS) is plotted for the low-spin (LS) and high-spin (HS) states of Ni^{3+} (d^7) doped $PbTiO_3$ (PTO). The PDOS is shown for the $2p$ states of the O ions, the $3d$ states of the Ti ions, as well as the t_{2g} and e_g states of the dopant. The PDOS has been shifted such that the Fermi energy is at zero in the plots.

simplification, as in reality some hybridization takes place with the O $2p$ states. As an example of the electronic structure for the doped $PbTiO_3$ systems under study, in Fig. 2 the partial and projected density of states (PDOS) is plotted for the LS and HS states of Ni^{3+}:PTO. As can be seen, the PDOS confirms the predicted orbital configurations from Table I.

It was originally proposed by Bersuker (Ref. [13]) that B-cations in a perovskite oxide will exhibit a different ferroelectric instability in different spin states; this effect provides a mechanism for the so-called multiferroic crossover effect, whereby switching the spin state of the B-cation could strongly affect the ferroelectric polarization, and vice versa. Recently, we have demonstrated that for $3d^4$–$3d^7$ B-cations, switching between a LS and HS state will strongly increase the ferroelectric lattice instability [11]. This multiferroic effect can be understood within the pseudo-Jahn-Teller (PJT) theory for ferroelectricity [13,27–29]; we summarize the key points below. Within the PJT theory, the lattice distortion is treated as a perturbation to the Hamiltonian (H) in the cubic phase, and the tendency for a BO_6 octahedron in a perovskite oxide to exhibit a ferroelectric distortion (Q) is described by the curvature in the potential energy surface (K) along Q. A negative curvature, i.e., $K < 0$, suggests a ferroelectric lattice instability. In this approach, K is expressed as the sum of two competing terms,

$$K = K_0 + K_v, \tag{1}$$

where

$$K_0 = \left\langle \Psi_0 \middle| \left(\frac{\delta^2 H}{\delta Q^2} \right)_0 \middle| \Psi_0 \right\rangle. \tag{2}$$

Within second-order perturbation theory, K_v is expressed as follows [13,27]:

$$K_v = -2 \sum_n \frac{\left| \langle \Psi_0 \left| \left(\frac{\delta H}{\delta Q} \right)_0 \right| \Psi_n \rangle \right|^2}{(E_0 - E_n)}. \tag{3}$$

Here, Ψ_0 is the ground-state wave function of the unperturbed system (at Q_0) with energy E_0, and Ψ_n are excited states with energy E_n. Whether or not a polar ferroelectric phase is favored depends on the relative strengths of the contributions K_0 and K_v in Eq. (1). The term K_0 described by Eq. (2) is always positive, and therefore K_0 provides a restoring force that favors the high symmetry phase. The term K_v is the so-called "vibronic term," which lowers the total energy as it corresponds to the response of the electronic wave function to the distortion, which is the mixing of Ψ_0 with appropriate excited states, Ψ_n. It is important to note that the matrix elements $\langle \Psi_0 | (\delta H / \delta Q)_0 | \Psi_n \rangle$ in Eq. (3) are only nonzero if Ψ_0 and Ψ_n have the same spin. It is this consideration that leads to the multiferroic crossover effect. Due to the denominator in Eq. (3) ($E_0 - E_n$), it is clear that a strong polar distortion requires that low-lying excited states exist, with the same spin-multiplicity as the ground state.

It has recently been shown that the K_0 term from Eq. (2) is strongly reduced with increasing volume [30]. For a d^4–d^7 B-cation in a perovskite oxide, the volume and B–O bond lengths are strongly increased in the HS state when compared to the LS state, and this is due to the population of the axial σ^* e_g states; we have recently demonstrated that the corresponding reduction in the K_0 term strongly enhanced the ferroelectric lattice instability [11]. Moreover, the vibronic term (K_v) is typically increased for the HS state of d^4–d^7 B-cations, and this further enhances the ferroelectric lattice instability in the HS state with respect to the LS configuration [11]. This is evident from Fig. 3, where the orbital configurations of the ground and lowest excited states are compared for a d^7 B-cation. For the LS state, the t_{2g} band is fully occupied; the e_g band is singly occupied, however promoting an electron into this band does not conserve the spin of the system. As a consequence, for the LS state, the lowest-lying excited states involving the t_{2g} and e_g bands do not contribute to the summation in Eq. (3), and a B-cation in this state is not expected to exhibit a strong ferroelectric instability [11,13]. On the other hand, for the HS state, the lowest excited states involving *both* the t_{2g} and e_g bands conserve the spin of the system, and so both excited states contribute to the summation in Eq. (3), and a B-cation in this state is expected to exhibit a strong driving force for a ferroelectric distortion [11,13]. Using a similar argument for other d^4–d^7 cations, one can predict that the HS state should exhibit a stronger ferroelectric instability than the LS state [11].

B. Multiferroic doping of $PbTiO_3$

We now investigate local spin-lattice coupling effects for magnetic TM ions embedded into the ferroelectric host

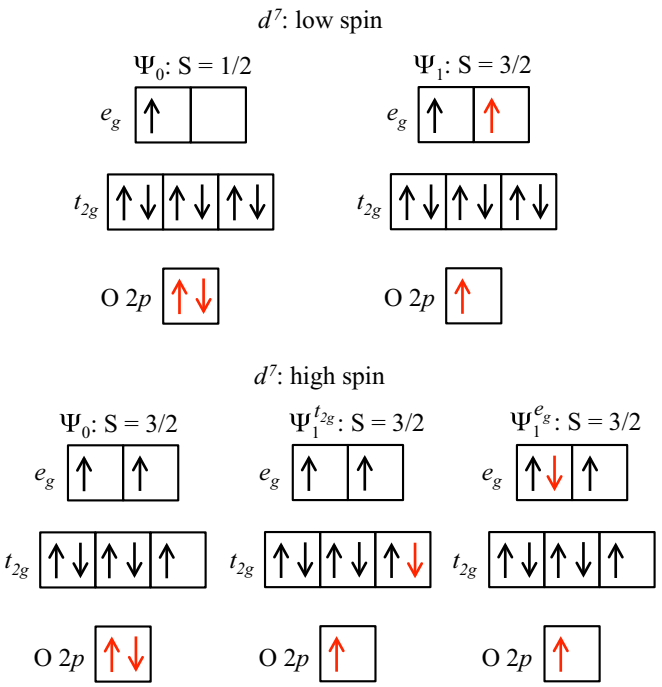

FIG. 3. The electron configurations of the ground state (ψ_0) and first excited states (ψ_1) for a low-spin (top) and high-spin (bottom) d^7 cation in a perovskite oxide. The labels $\psi_1^{t_{2g}}$ and $\psi_1^{e_g}$ indicate the lowest excited state involving the t_{2g} and e_g bands, respectively. For the low-spin state, ψ_0 has a total spin $S = 1/2$, whereas for ψ_1 an electron has been promoted from the O 2p band into the majority-spin channel of the e_g band. The total spin of ψ_1 is $S = 3/2$, and therefore spin is not conserved and a cation in this state is not expected to be ferroelectric. For the high-spin state, ψ_0 has $S = 3/2$, and excitation of an electron into the t_{2g} or e_g bands conserves the spin of the system. Therefore, high-spin d^7 B-cations are more likely to be ferroelectric.

material PTO. The same or similar systems, including Co and Fe doped PTO (and BTO), have been fabricated recently by experiment [31–35]. We have performed these calculations at both the GGA (PBE) and hybrid HSE06 level; interestingly, we find that the calculated geometries are not significantly affected by the choice of functional, i.e., the geometries are not affected by the HSE mixing parameter (as will be discussed in Sec. III C, the spin-state energetics *are* affected by the mixing parameter). We perform fixed-spin moment calculations, which allow us to force the dopant atom into either a LS, IS, or HS state—the local geometries around the dopants in different spin and charge states are presented in Table II (the preferred charge state will depend on growth conditions [36]). The presented results are calculated using the HSE06 functional. It is found that spin-lattice coupling effects manifest as changes in the local ferroelectric character of the bonding environment surrounding the dopant; namely, spin crossover can induce a shift (along the [001] direction) of the dopant ion with respect to the oxygen ions in the surrounding octahedron. In a perovskite oxide, the B-site cation has two TM–O bonds along the c axis, which are referred to as the [001] and [00$\bar{1}$] bonds, respectively. For a cubic perovskite, these two bonds have the same length. On the other hand, for a tetragonal perovskite with ferroelectric distortions, due to the shifting of

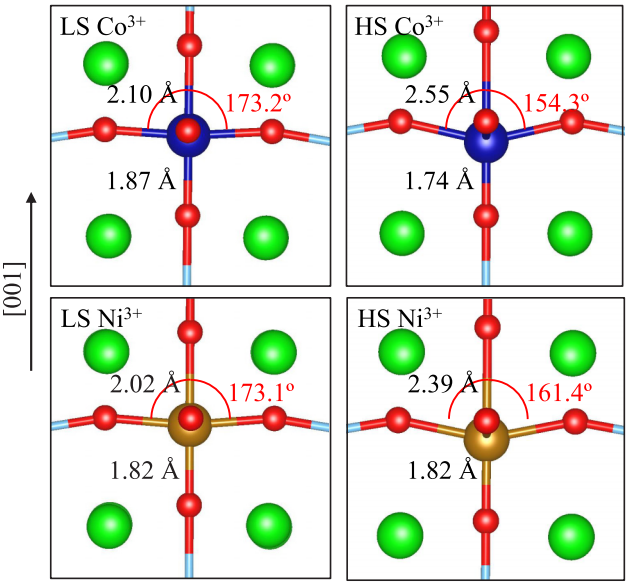

FIG. 4. Local distortions around the dopant induced by spin crossover. Geometries are shown for a Co^{3+} ion in the low-spin (top left) and high-spin (top right) states, as well as for a Ni^{3+} ion in the low-spin (bottom left) and high-spin (bottom right) states. The [001] and [00$\bar{1}$] TM–O bond lengths and the [100] O–TM–O bond angles are indicated. Pb atoms are shown in green, O are red, Co are blue, and Ni are gold.

the B-cation with respect to surrounding oxygen, one of these bonds is lengthened while the other is shortened. Therefore, to quantify the spin-lattice coupling effects observed, in Table II the TM–O c-axis bond lengths are presented. Also presented are the [100] O–TM–O bond angles—for a cubic structure this angle is 180°, and so a reduction of this bond angle represents a shift of the dopant with respect to the surrounding O_6 octahedron (which represents a local ferroelectric-like distortion). These quantities are shown in Fig. 4, where we identify the relevant bond lengths and bond angle, shown as an example for LS and HS Co^{3+} and Ni^{3+} dopants.

From Table II, it is clear that a systematic trend for spin-lattice coupling is observed. In each case, the local coordinates in the LS state more closely resemble those of a paraelectric system: for example, for the case of Co^{3+}:PTO the [001] and [00$\bar{1}$] Co–O bond lengths are similar, namely 2.10 and 1.87 Å, respectively. Additionally, the [100] O–Co–O bond angle is 173.2°, close to the 180° expected for the tetragonal symmetry without internal distortions. In contrast, for the HS state, the structure exhibits strong ferroelectric-like distortions characterized by the displacement of the dopant ion with respect to the surrounding O_6 octahedral cage. This effect is exemplified by the variation in the c-axis Co–O bond lengths. The [001] Co–O bond is significantly elongated to 2.55 Å, whereas the [00$\bar{1}$] bond is shortened to 1.74 Å. The [100] O–Co–O bond angle also decreases to 154.3°—a significant deviation from the LS structure. The results are qualitatively the same for Ni^{3+}:PTO; in Table II, the TM–O bond lengths and O–TM–O bond angles are presented for the LS, IS, and HS states of each of the d^4–d^7 dopants under study. Clearly, an obvious trend is observed for an increased ferroelectric-like

TABLE II. Local distortions around the dopant in transition-metal (TM) doped $PbTiO_3$ in the low-spin (LS), intermediate-spin (IS), and high-spin (HS) states. The distortions are characterized by the TM–O [001] bond lengths, and the O–TM–O [100] bond angle. As shown in Fig. 4, a reduction in the O–TM–O [100] bond angle, and a shortening of one TM–O [001] bond at the expense of the other, is indicative of a ferroelectric-like distortion. Also included is the energy of each spin state, referenced to the total energy of the HS state (a positive value indicates that the HS state is preferred).

			Bond length (Å)		Bond angle (deg)	
TM	d^n	Spin	TM–O [001]	TM–O [00$\bar{1}$]	O–TM–O [100]	Energy (eV)
Mn^{3+}	d^4	LS	2.17	1.82	168.7	0.915
		HS	2.41	2.08	165.2	0.000
Mn^{2+}	d^5	LS	2.14	1.82	169.9	1.485
		IS	2.40	2.07	165.7	0.708
		HS	2.51	2.01	156.6	0.000
Fe^{3+}	d^5	LS	2.07	2.03	176.9	1.357
		IS	2.32	2.05	155.1	0.803
		HS	2.52	1.91	155.8	0.000
Fe^{2+}	d^6	LS	2.12	1.86	172.2	1.304
		IS	2.45	1.92	161.4	1.211
		HS	2.49	1.85	157.3	0.000
Co^{4+}	d^5	LS	2.11	1.74	170.9	−0.006
		IS	2.48	1.76	158.6	0.054
		HS	2.45	1.74	158.5	0.000
Co^{3+}	d^6	LS	2.10	1.87	173.2	0.350
		IS	2.41	1.96	164.9	1.008
		HS	2.55	1.74	154.3	0.000
Co^{2+}	d^7	LS	2.32	2.15	179.3	0.085
		HS	2.47	1.94	159.3	0.000
Ni^{4+}	d^6	LS	2.08	1.82	172.9	−0.428
		IS	2.30	1.97	168.3	−0.078
		HS	2.38	1.82	161.4	0.000
Ni^{3+}	d^7	LS	2.02	1.82	173.1	0.003
		HS	2.39	1.82	161.4	0.000

distortion in the HS state, when compared to the LS (or IS) states. Therefore, it is concluded that, in principle, the multiferroic crossover effect is a general property of d^4–d^7 dopants in ferroelectric materials.

The origin of the large spin-lattice coupling is the multiferroic crossover effect [13], as discussed in Sec. III A. The increased ferroelectric distortion in the HS state can be thought of as being driven by increased *p-d* covalent bonding. This idea is supported by the spin-density isosurface plots presented in Fig. 5 for the LS and HS states of Co^{3+}:PTO and Ni^{3+}:PTO. As can be seen, for both ions in the HS state a large portion of the spin density can be seen on the apical oxygen below the magnetic B-cation. For example, for LS Ni^{3+}:PTO, the spin density is localized on the Ni^{3+} ion; in the HS state, a large spin density is seen on the apical O ion, indicating an increased *p-d* hybridization.

Before moving forward, we make some comments here about the experimental realization and characterization of the doped multiferroics considered in this work. We have investigated isolated dopants, i.e., the dilute limit, where the interactions between dopants can be neglected. We suggest that this type of doping can be achieved via ion implantation [37]; indeed, implanted TM ions form isolated paramagnetic centers when substituting at the Ti^{4+} site in $BaTiO_3$ [38]. Even more ideally, advanced doping techniques based on scanning tunneling microscopy have recently allowed the placement, as well as manipulation and characterization, of individual dopants with atomic precision [39]; this would also open up the possibility to study the magnetic coupling between

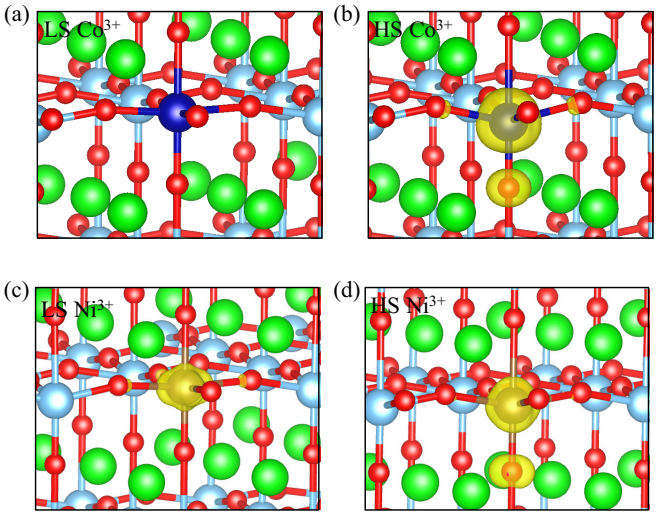

FIG. 5. Spin-density isosurface plots for low-spin (LS) Co^{3+}:$PbTiO_3$ (a), high-spin (HS) Co^{3+}:$PbTiO_3$ (b), LS Ni^{3+}:$PbTiO_3$ (c), and HS Ni^{3+}:$PbTiO_3$ (d). The isosurface value is set to 10% of the maximum value.

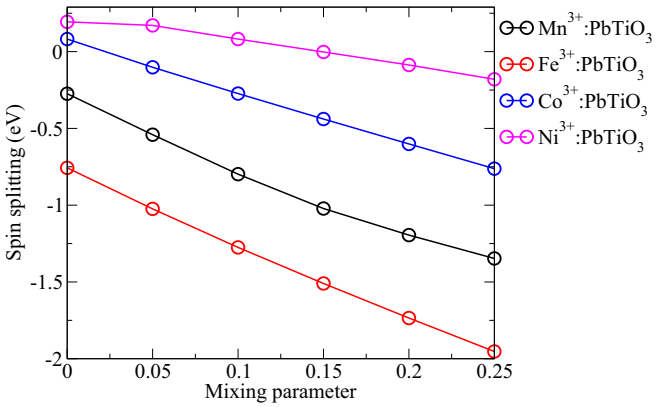

FIG. 6. The high-spin (HS)–low-spin (LS) splitting is plotted for d^4–d^7 dopants in $PbTiO_3$ as a function of the mixing parameter used in the hybrid functional calculation. A negative value means that the HS state is preferred compared to the LS state.

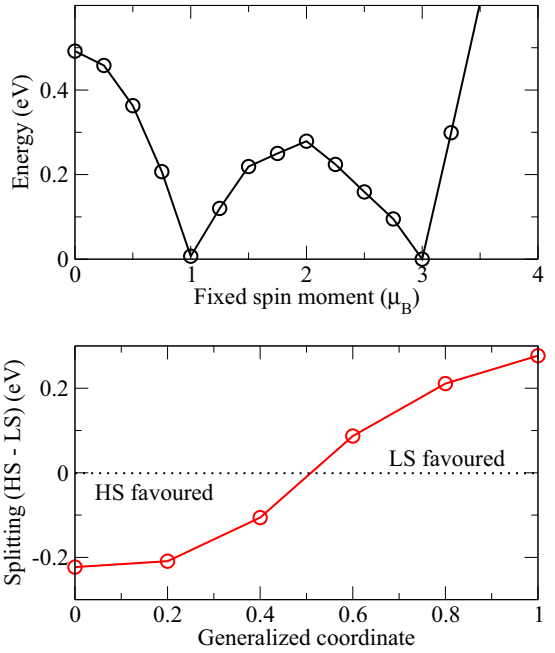

FIG. 7. Top: The total energy of Ni^{3+}:$PbTiO_3$ is plotted as a function of the fixed spin moment in the supercell. Bottom: The difference in the total energy of low-spin (LS) and high-spin (HS) Ni^{3+}:$PbTiO_3$ is plotted as a function of the internal ferroelectric polarization. Starting at the relaxed HS geometry (generalized coordinate = 0), the system is moved such that the internal coordinates reflect a paraelectric structure (generalized coordinate = 1). A negative value of the curve implies the HS state is the magnetic ground state, a positive value implies that the LS state is preferred.

individual dopants. The dopant-dopant magnetic interaction modulated via the multiferroic crossover effect, as well as the superexchange interaction [40], could lead to even more novel magnetoelectric effects [41], however this is outside the scope of the present paper. Finally, in order to characterize multiferroic and spin crossover at individual dopants in these systems, x-ray spectroscopy, such as x-ray magnetic circular dichroism (XMCD), will be ideal to characterize the magnetic structure of the doped ions [42]; moreover, Raman spectroscopy has been shown to be an ideal technique to reveal the softening of local vibrational modes associated with a ferroelectric lattice instability on a microscopic scale [43].

C. The effect of exact exchange

As was discussed, the spin-lattice coupling effects from the previous section were insensitive to the choice of mixing parameter in HSE calculations. However, we find that the spin splitting is highly sensitive to the mixing parameter. To demonstrate this, in Fig. 6 the HS-LS splitting is plotted for Mn^{3+}, Fe^{3+}, Co^{3+}, and Ni^{3+}, as representative examples of d^4–d^7 systems, as a function of the HSE mixing parameter. As can be seen, upon increasing the mixing fraction from $\alpha = 0$ to 0.25, the HS state is systematically favored. For a mixing fraction of 25% (HSE06), all of the dopants are found to prefer the HS state. Moreover, the variations are very large; for example, for Fe^{3+}:PTO the HS-LS splitting varies by about 1.5 eV going from $\alpha = 0$ (pure GGA) to $\alpha = 0.25$ (HSE06).

This type of large variation has been reported before for d^4–d^7 spin-crossover ions in transition-metal complexes. In fact, systematic studies in some molecular magnets, where the predicted ground spin state from hybrid functional calculations is compared with known experimental data, have revealed that the GGA systematically favors the LS state, whereas hybrid calculations with standard 20–25 % mixing will systematically (and often erroneously) favor the HS state [21,22]. For the local and semilocal functionals (LDA/GGA), the tendency to favor the LS state originates from the self-interaction error, which leads to a delocalization of transition-metal d orbitals, spuriously increasing the crystal-field splitting. On the other hand, standard hybrid functionals with 25% mixing suffer from the same tendency to favor the HS state as pure Hartree-Fock calculations, and this originates from the inclusion of exact exchange without a proper treatment of dynamic correlation [22]. Studies of molecular magnets reveal that by reducing the mixing parameter to within the range of 10–15 %, the experimental ground spin state is well reproduced [21,22].

In Table II, we list the spin-splitting for each d^4–d^7 ion studied. To calculate the splitting, we use a mixing parameter of 12.5%, the midpoint of the recommended range from Refs. [21,22]. It can be seen that, in some cases, there exist excited spin states with an energy only slightly higher than the ground state—this suggests magnetic metastability, and the potential for spin crossover [26,44]. Moreover, due to the large spin-lattice coupling of these dopants, this might provide a mechanism for strong magnetoelectric coupling [11,16].

D. Spin switching

As was shown in the previous section, certain cations exhibit a magnetic bistability, where two spin states have a similar energy but with markedly different geometries. For example, Ni^{3+}:PTO has a HS ground state, however the LS state is calculated to be only 3 meV higher in energy. This is confirmed in Fig. 7, where we plot a fixed spin moment (FSM) curve for Ni^{3+}; here, the total energy of the supercell is calculated as a function of a constrained magnetic moment. As can be seen, the FSM curve exhibits a deep double-well profile, with minima on the energy curve corresponding to the

LS and HS states. This type of FSM curve does indeed predict magnetic bistability [16,26]

The large conformational changes in the local structure induced by spin crossover for these dopants has important consequences from an applications perspective. The key requirement of spin crossover materials is magnetic bistability, and it is therefore important that the excited state is metastable and with a finite lifetime after switching, e.g., by an applied laser. We find that the relaxation energies associated with the different spin states of each dopant are significant. For example, in Co^{3+}:PTO the HS state is the ground state by 350 meV (compared to the LS state), however at the relaxed LS geometry the LS state has a lower energy by 284 meV—since the LS state is the ground state at these coordinates, if a Co^{3+} in PTO is in the LS state, energy must be put into the system so as to relax back to the ground state. This suggests that the metastable LS state would indeed be stable, or even possibly that switching would be nonvolatile.

As seen above, the changes in the local geometry surrounding the dopant induced by switching the spin state are ferroelectric in nature—this immediately suggests the potential for magnetoelectric coupling. The internal polarization of a ferroelectric can be manipulated by the application of an electric field, and the dielectric response is primarily characterized by the displacement of the B-cation with respect to the O ions in the surrounding octahedron (similar to what is seen in Fig. 4). Focusing on Ni^{3+}:PTO (which has the smallest HS-LS splitting), the ground state is the HS state; however, an appropriately applied external field would reduce the internal polarization, the dopant ion would move in a direction opposite to the surrounding O ions, and the local coordinates could be modified to more closely resemble the LS coordinates—this could change the relative energies of the LS and HS states and lead to an electric-field-induced spin crossover. To demonstrate this effect, in Fig. 7 the HS-LS splitting is plotted starting from the relaxed geometry of HS Ni^{3+}:PTO (generalized coordinate = 0), and to mimic the effect of an applied electric field, the internal coordinates are slowly moved to that of a paraelectric structure (generalized coordinate = 1). Initially, the HS state has a lower energy, but as the system is moved toward a paraelectric structure, the LS state becomes the magnetic ground state. This suggests that the multiferroic crossover effect could provide a new route to electric field manipulation of magnetism in the magnetic doped PTO systems.

IV. CONCLUSIONS

Using first-principles calculations, we have studied local spin-lattice coupling effects at isolated $3d^4$–$3d^7$ TM ions doped into nonmagnetic, ferroelectric PTO. A general trend was found for increased local ferroelectric character around the dopant in the HS state, when compared to the LS state, and we have explained this in terms of the PJT theory for ferroelectricity. Importantly, this multiferroic crossover effect is a general property of d^4–d^7 TM ions when doped into a ferroelectric host material. Finally, it was proposed that, since spin crossover can lead to a change in the local electrical polarization, the application of an electric field could potentially lead to spin crossover. Test calculations supported this hypothesis. We suggest that this single-atomic multiferroic crossover effect in semiconductor solid solution could lead to novel spintronics and solotronics applications.

ACKNOWLEDGMENTS

We gratefully acknowledge computational resources provided by the Australian National Computational Infrastructure (NCI), and support from the Australian Research Council.

[1] R. Ramesh and N. A. Spaldin, Nat. Mater. **6**, 21 (2007).
[2] S.-W. Cheong, Nat. Mater. **6**, 927 (2007).
[3] C.-W. Nan, M. I. Bichurin, S. Dong, D. Viehland, and G. Srinivasan, J. Appl. Phys. **103**, 031101 (2008).
[4] A. Roy, R. Gupta, and A. Garg, Adv. Condens. Matter Phys. **2012**, 926290 (2012).
[5] M. Gajek, M. Bibes, S. Fusil, K. Bouzehouane, J. Fontcuberta, A. Barthelemy, and A. Fert, Nat. Mater. **6**, 296 (2007).
[6] F. Yang, M. H. Tang, Z. Ye, Y. C. Zhou, X. J. Zheng, J. X. Tang, J. J. Zhang, and J. He, J. Appl. Phys. **102**, 044504 (2007).
[7] M. Bibes and A. Barthelemy, Nat. Mater. **7**, 425 (2008).
[8] J. F. Scott, Nat. Mater. **6**, 256 (2007).
[9] R. E. Cohen, Nature (London) **358**, 136 (1992).
[10] N. A. Hill, J. Phys. Chem. B **104**, 6694 (2000).
[11] L. Weston, X. Y. Cui, S. P. Ringer, and C. Stampfl, Phys. Rev. B **93**, 165210 (2016).
[12] D. Khomskii, J. Magn. Magn. Mater. **306**, 1 (2006).
[13] I. B. Bersuker, Phys. Rev. Lett. **108**, 137202 (2012).
[14] N. A. Benedek and C. J. Fennie, J. Phys. Chem. C **117**, 13339 (2013).
[15] U. Aschauer and N. A. Spaldin, J. Phys. Condens. Matter **26**, 122203 (2014).
[16] L. Weston, X. Y. Cui, S. P. Ringer, and C. Stampfl, Phys. Rev. Lett. **114**, 247601 (2015).
[17] P. M. Koenraad and M. E. Flatté, Nat. Mater. **10**, 91 (2011).
[18] C. G. Yale, B. B. Buckley, D. J. Christle, G. Burkard, F. J. Heremans, L. C. Bassett, and D. D. Awschalom, Proc. Natl. Acad. Sci. (USA) **110**, 7595 (2013).
[19] J. Heyd, G. Scuseria, and M. Ernzerhof, J. Chem. Phys. **118**, 8207 (2003).
[20] J. P. Perdew, K. Burke, and M. Ernzerhof, Phys. Rev. Lett. **77**, 3865 (1996).
[21] J. N. Harvey, in *Principles and Applications of Density Functional Theory in Inorganic Chemistry I* (Springer, Berlin, Heidelberg, 2004), pp. 151–184.
[22] M. Reiher, O. Salomon, and B. A. Hess, Theor. Chem. Acc. **107**, 48 (2001).
[23] P. E. Blöchl, Phys. Rev. B **50**, 17953 (1994).
[24] G. Kresse and J. Furthmüller, Phys. Rev. B **54**, 11169 (1996).
[25] Y. Kuroiwa, S. Aoyagi, A. Sawada, J. Harada, E. Nishibori, M. Takata, and M. Sakata, Phys. Rev. Lett. **87**, 217601 (2001).
[26] X. Y. Cui, B. Delley, A. J. Freeman, and C. Stampfl, Phys. Rev. Lett. **97**, 016402 (2006).

[27] I. B. Bersuker, *The Jahn-Teller Effect* (Cambridge University Press, Cambridge, U.K., 2006).
[28] I. B. Bersuker, Chem. Rev. **113**, 1351 (2013).
[29] V. Polinger, P. Garcia-Fernandez, and I. Bersuker, Physica B **457**, 296 (2015).
[30] J. García-Lastra, P. García-Fernández, F. Calle-Vallejo, A. Trueba, J. Aramburu, and M. Moreno, Inorg. Chem. **53**, 6534 (2014).
[31] Y.-H. Lin, S. Zhang, C. Deng, Y. Zhang, X. Wang, and C.-W. Nan, Appl. Phys. Lett. **92**, 112501 (2008).
[32] L. Gao, J. Zhai, and X. Yao, Appl. Surf. Sci. **255**, 4521 (2009).
[33] Z. Ren, G. Xu, X. Wei, Y. Liu, X. Hou, P. Du, W. Weng, G. Shen, and G. Han, Appl. Phys. Lett. **91**, 063106 (2007).
[34] S. Ray, P. Mahadevan, S. Mandal, S. R. Krishnakumar, C. S. Kuroda, T. Sasaki, T. Taniyama, and M. Itoh, Phys. Rev. B **77**, 104416 (2008).
[35] V. Palkar and S. Malik, Solid State Commun. **134**, 783 (2005).
[36] H.-J. Hagemann and D. Hennings, J. Am. Ceram. Soc. **64**, 590 (1981).
[37] T. Shinada, S. Okamoto, T. Kobayashi, and I. Ohdomari, Nature (London) **437**, 1128 (2005).
[38] S. Kazan, F. A. Mikailzade, A. G. Şale, M. Maksutoğlu, M. Acikgoz, R. I. Khaibullin, N. I. Khalitov, J. I. Gatiiatova, and V. F. Valeev, Phys. Rev. B **82**, 054402 (2010).
[39] M. Fuechsle, J. A. Miwa, S. Mahapatra, H. Ryu, S. Lee, O. Warschkow, L. C. Hollenberg, G. Klimeck, and M. Y. Simmons, Nat. Nanotechnol. **7**, 242 (2012).
[40] J. Kanamori, J. Phys. Chem. Solids **10**, 87 (1959).
[41] J. Hong, A. Stroppa, J. Íniguez, S. Picozzi, and D. Vanderbilt, Phys. Rev. B **85**, 054417 (2012).
[42] M. W. Haverkort, Z. Hu, J. C. Cezar, T. Burnus, H. Hartmann, M. Reuther, C. Zobel, T. Lorenz, A. Tanaka, N. B. Brookes *et al.*, Phys. Rev. Lett. **97**, 176405 (2006).
[43] D. Lee, H. Lu, Y. Gu, S.-Y. Choi, S.-D. Li, S. Ryu, T. Paudel, K. Song, E. Mikheev, S. Lee *et al.*, Science **349**, 1314 (2015).
[44] P. Gutlich and H. Goodwin, in *Spin Crossover in Transition Metal Compounds I*, Topics in Current Chemistry Vol. 233 (Springer, Berlin, 2004).